Physica Medica 114 (2023) 102661

Contents lists available at ScienceDirect

Physica Medica

journal homepage: www.elsevier.com/locate/ejmp

Calculation of electron interaction models in N_2 and O_2

F. Nicolanti [a,b,*], B. Caccia [c], A. Cartoni [d], D. Emfietzoglou [e], R. Faccini [a,b], S. Incerti [f], I. Kyriakou [e], M. Satta [d,g], H.N. Tran [f], C. Mancini-Terracciano [a,b]

[a] Physics Dep., Sapienza U. of Rome, p.le Aldo Moro, 5, 00185, Rome, Italy
[b] INFN, Sec. of Rome, p.le Aldo Moro, 2, 00185, Rome, Italy
[c] ISS(Italian National Institute of Health), V. Regina Elena, 299, 00161, Rome, Italy
[d] Chemistry Dep., Sapienza U. of Rome, p.le Aldo Moro, 5, 00185, Rome, Italy
[e] Med. Phys. Lab., Dept of Medicine, University of Ioannina, 45110, Ioannina, Greece
[f] Université de Bordeaux, CNRS, LP2I Bordeaux, UMR 5797, Chemin du Solarium, 19, 33170, Gradignan, France
[g] ISMN-CNR, p. Aldo Moro, 7, 00185, Rome, Italy

ARTICLE INFO

Keywords:
Electron cross sections
Atmosphere ionization
Particle track structure
Monte Carlo simulation
Geant4-DNA

ABSTRACT

Cosmic rays have the potential to significantly affect the atmospheric composition by increasing the rate and changing the types of chemical reactions through ion production. The amount and states of ionization, and the spatial distribution of ions produced are still open questions for atmospheric models. To precisely estimate these quantities, it is necessary to simulate particle–molecule interactions, down to very low energies. Models enabling such simulations require interaction probabilities over a broad energy range and for all energetically allowed scattering processes.

In this paper, we focus on electron interaction with the two most abundant molecules in the atmosphere, i.e., N_2 and O_2, as an initial step. A set of elastic and inelastic cross section models for electron transportation in oxygen and nitrogen molecules valid in the energy range 10 eV – 1 MeV, is presented. Comparison is made with available theoretical and experimental data and a reasonable good agreement is observed. Stopping power is calculated and compared with published data to assess the general consistency and reliability of our results. Good overall agreement is observed, with relative differences lower than 6% with the ESTAR database.

1. Introduction

The emission of polluting molecules and greenhouse gases into the atmosphere represents a global challenge with open scientific questions, mainly related to the approximation grade of chemical–physical processes used in the prevision models of climate change. Although ions play a pivotal role in various atmospheric processes such as ion-induced nucleation, precipitation, and aerosol formation, the influence of cosmic rays and ions on climate is at the dawn of a full understanding and deserves further in-depth investigations [1].

Chemical reaction rates can vary by up to 10 orders of magnitude depending on the ionization state of the involved species [2,3]. Thus, cosmic rays ionization could significantly impact chemical reactions in the atmosphere, considering also that the ions produced are clustered near the primary ray. The amount and state of ionization, as well as the spatial distribution of ions in the atmosphere, are open questions for the atmospheric models, that it is fundamental to investigate also in the very low-energy range [4–6].

Oxygen and nitrogen molecules are the two most prevalent species in Earth's troposphere and lower stratosphere. Therefore, studying the interaction of cosmic rays with these molecules is crucial for our understanding of various atmospheric phenomena. For instance, electron impact ionization plays a role in the inter-conversion between ozone and oxygen in the atmosphere, while nitrogen is involved in the production of one of the most dangerous greenhouse gasses: nitrous oxide [7–9]. The ejection of secondary electrons in collisions with individual molecules represents the elementary process involving the greatest energy transfer and is of central interest in any study concerning the interaction of charged particles with matter. For large energy ranges, it is also the most likely process.

Event-by-event simulations are a powerful tool for studying the details of radiation-induced effect at the molecular level. Nowadays, several existing Monte Carlo track-structure (MC-TS) codes fulfill this purpose. One of these is Geant4-DNA [10–13], an extension of Geant4 (GEometry ANd Tracking) [14–16] which is the most widely used toolkit for performing MC simulations of radiation–matter interactions. Geant4-DNA makes it possible to explicitly simulate every single electromagnetic particle interaction down to low energy (about 10 eV), as

* Corresponding author at: Physics Dep., Sapienza U. of Rome, p.le Aldo Moro, 5, 00185, Rome, Italy.
E-mail address: francesca.nicolanti@uniroma1.it (F. Nicolanti).

https://doi.org/10.1016/j.ejmp.2023.102661
Received 14 February 2023; Received in revised form 19 June 2023; Accepted 5 August 2023
Available online 11 September 2023

well as diffusion and chemical reactions, on some specific materials of interest in radiobiology [17,18].

The aim of this work is to provide a comprehensive and reliable set of electron impact electromagnetic interaction models for O_2 and N_2 molecules down to the 10 eV scale, for use in such simulation code. This will allow to accurately simulate the interaction of low-energy secondary radiation with molecules, the exact concentration of ions produced, their spatial distribution, and the ionization state.

We selected a model for each relevant electromagnetic electron impact interaction process in the energy range 10 eV – 1 MeV, including ionization, electronic excitation, and elastic scattering. Given the computational constraints of a simulation code, we focused on choosing calculation methods that are both sustainable and efficient. In this regard, models that provide an analytical expression for the cross section and a good compromise between accuracy and computational time were preferred. The physics models presented here can be easily adapted to be used for molecules in the gas phase and further work is planned to extend them to other species of climate interest. One of these is the trace gas SO_2, studied at CERN in the CLOUD experiment [19,20], which has proven to have large effects on ozone chemistry.

The selected models are briefly described in Section 2. In Section 3, we present the benchmark of our models implementation. Specifically, in Section 3.1, we show the partial cross sections obtained for each process and compare them with experimental data or other calculations. In Section 3.2, we provide a final validation by comparing the calculated stopping power, obtained using the selected models, with semi-empirical results and ab-initio calculations. The stopping power is also compared with the ICRU (International Commission on Radiation Units and Measurements) recommended values calculated by ESTAR available down to 1 keV, which are a good benchmark for MC calculations. The ESTAR values have uncertainties ranging from 1% to 2% (in low-Z materials), for energies higher than 10 keV. These uncertainties grow up to 10% at 1keV, due to the omission of shell corrections [21].

2. Description of physics models

2.1. Ionization

Electron impact ionization is based on the Relativistic Binary Encounter Bethe (RBEB) model [22], which combines the relativistic Mott cross section, known as the Møller cross section, with the relativistic version of the Bethe cross section. It represents the high-energy extension of the corresponding Binary Encounter Bethe model developed by Kim and Rudd [23].

Within the framework of this model, the energy differential cross section (DCS) $\frac{d\sigma_{MO}(t)}{dw}$ with the energy of the ejected electron W at a given incident energy T for a molecular orbital (MO), can be written as

$$\frac{d\sigma_{MO}}{dw} = \frac{4\pi a_0^2 \alpha^4 N}{\left(\beta_t^2+\beta_u^2+\beta_b^2\right)2b'}\left[-\frac{1}{t+1}\left(\frac{1}{w+1}+\frac{1}{t-w}\right)\times\frac{1+2t'}{(1+t'/2)^2} + \frac{1}{(w+1)^2}+\frac{1}{(t-w)^2}+\frac{b'}{(1+t'/2)^2}+\left(\ln\left(\frac{\beta_t^2}{1-\beta_t^2}\right)-\beta_t^2-\ln\left(2b'\right)\right) \times\left(\frac{1}{(w+1)^3}+\frac{1}{(t-w)^3}\right)\right] \tag{1}$$

where

$$t = T/B, \quad w = W/B, \quad u = U/B$$

$$\beta_t^2 = 1-\frac{1}{(1+t')^2}, \quad t' = T/m_e c^2$$

$$\beta_u^2 = 1-\frac{1}{(1+u')^2}, \quad u' = U/m_e c^2$$

$$\beta_b^2 = 1-\frac{1}{(1+b')^2}, \quad b' = B/m_e c^2$$

The RBEB formula depends only on the three input parameters, i.e. the binding energy (B), the mean kinetic energy (U) and the occupancy number (N) of each molecular orbital. The simple analytical form in Eq. (1) is ideally suited for modeling applications and Monte Carlo simulation as it allows energy loss to be randomly sampled during an ionization event without the need for lengthy cross sections tables [24].

This model is valid for electron energies that are significantly higher than the binding energy of the target electron, as it is based on the First Born Approximation. Nevertheless, for many stable molecules including N_2 and O_2, it yields ionization cross sections that are in good agreement in both magnitude (with deviations of 15% or less at the peak) and shape from each shell ionization threshold onwards [25,26]. We have imposed the high-energy limit to 1 MeV, as for higher energies other relativistic effects, such as the density effect, must be considered.

In the RBEB model the scattering angle of the primary electron and the ejected angle of the secondary electron are assumed to be isotropic. This approximation can be reduced by introducing a sampling of both angles determined by the kinematics of binary collisions [27].

The ionization cross section for each molecular orbital is given by integration of Eq. (1) up to the maximum energy of the ejected electron $W_{max} = (T-B)/2$, namely,

$$\sigma_{MO}^{Ioni} = \frac{4\pi a_0^2 \alpha^4 N}{(\beta_t^2+\beta_u^2+\beta_b^2)2b'}\times\left\{\frac{1}{2}\left[\ln\left(\frac{\beta_t^2}{1-\beta_t^2}\right)-\beta_t^2-\ln(2b')\right]\times\left(1-\frac{1}{t^2}\right) + 1-\frac{1}{t}-\frac{\ln t}{t+1}\frac{1+2t'}{(1+t'/2)}+\frac{b'^2}{(1+t'/2)^2}\frac{t'-1}{2}\right\} \tag{2}$$

For single ionization of inner k-shells which are subject to stronger nuclear attraction, we use the averaged RBEB formula [22,28]:

$$\sigma_{k-shell}^{Ioni} = \frac{1}{2}\left(1+\frac{\beta_t^2+\beta_u^2+\beta_b^2}{\beta_t^2}\right)\times\sigma_{MO}^{Ioni} \tag{3}$$

For oxygen molecules there are five outer shells and the inner K-shell of the oxygen atom, while for nitrogen molecules there are four outer shells plus the inner K-shell of the nitrogen atom. For each outer shell, the binding energies and the mean kinetic energies are from Hwang et al. [29], while K-shells parameters for diatomic molecules are from Jolly et al. [30] (Table 1).

2.2. Elastic scattering

Elastic scattering, although involving only minimal energy loss, strongly influences the accuracy of the spatial distribution of energy deposition.

To calculate the differential and integral elastic cross sections we used the IAM-SCAR method, which is based on the Independent Atom Model representation (IAM) [31] complemented with a Screening-Corrected Additivity Rule (SCAR) [32,33]. This method has already been extensively employed to calculate electron-scattering cross sections for a wide variety of molecular targets, over a broad energy range [34–38].

Under the IAM approximation, the scattering from a molecule is described by the direct and spin-flip scattering amplitudes:

$$F(\theta) \approx \sum f_i(\theta) e^{i\mathbf{q}\cdot r_i} \qquad \text{and} \qquad G(\theta) \approx \sum g_i(\theta) e^{i\mathbf{q}\cdot r_i} \tag{4}$$

where $q = k_f - k_i$ is the momentum transfer, r_i are the atomic positions, and $f_i(\theta)$ and $g_i(\theta)$ are the atomic scattering amplitudes. By averaging the modulus squared of the scattering amplitudes $|F(\theta)|^2$ and $|G(\theta)|^2$

Table 1
Required set of parameters for the calculation of ionization cross sections in molecular nitrogen and oxygen with the RBEB model.

	Ionization			
	Molecular Orbital	Threshold B (eV)	Mean kinetic energy U (eV)	N
N_2	$2\sigma_g$	41.72	71.13	2
	$2\sigma_u$	21.00	63.18	2
	$1\pi_u$	17.07	44.30	4
	$3\sigma_g$	15.58	54.91	2
	k-shell	409.5	603.3	4
O_2	$2\sigma_g$	46.19	79.73	2
	$2\sigma_u$	29.82	90.92	2
	$1\pi_u$	19.64	59.89	4
	$3\sigma_g$	19.79	71.84	2
	$1\pi_g$	12.07	84.88	2
	k-shell	543.8	796.2	4

over all molecule orientations [2, 6], we obtain the differential elastic cross section:

$$\frac{d\sigma^{elastic}_{molecule}}{d\Omega} = \sum_{i,j}\left[f_i(\theta)f_j^*(\theta)+g_i(\theta)g_j^*(\theta)\right]\frac{\sin(qr_{ij})}{qr_{ij}} = \sum_i\left[|f_i(\theta)|^2+|g_i(\theta)|^2\right] + \sum_{i\neq j}\left[f_i(\theta)f_j^*(\theta)+g_i(\theta)g_j^*(\theta)\right]\frac{\sin(qr_{ij})}{qr_{ij}} = \sum_i\frac{d\sigma^{elastic}_{atom\ i}}{d\Omega}+\frac{d\sigma^{interference}}{d\Omega} \tag{5}$$

where $q \equiv |\mathbf{q}| = 2k\sin(\theta/2)$ and r_{ij} is the distance between the i and j atoms. By integrating (5), the total molecular cross section can be written as:

$$\sigma^{IAM}_{molecule} = \sum_i \sigma_i + \sigma^{interference} = \sigma^{AR} + \sigma^{interference} \tag{6}$$

The first term σ^{AR} corresponds to the direct sum of atomic cross sections and it is equivalent to the molecular cross sections according to the Additivity Rule (AR) [39]. The second term $\sigma^{interference}$ represents the interference contribution between two single scattering events. Its main effect is to increase the differential cross sections at small scattering angles ($\theta < 30°$), leading to an overall increase in the integral cross section values. It must be noted that the second contribution would not be present in (6) if this expression were directly obtained from (4) by applying the optical theorem. Thus, differential cross sections should be renormalized to avoid inherent contradictions [35,36].

The above expressions are applicable for independent scattering from each atom and they are only valid for large interatomic distances compared to the wavelength associated with the incident electron ($\sim<$ 200 eV for N_2 and O_2). To extend their applicability to lower energies, the SCAR method introduces screening coefficients (s_i) in Eqs. (5)–(6). These coefficients have the effect to reduce the contribution of each atom to the overall molecular cross section ($0 \leq s_i \leq 1$) in the low energy range. Further details on these coefficients can be found elsewhere [32,33,40].

Atomic scattering amplitudes and cross sections in (5) were calculated using the ELSEPA (ELastic Scattering of Electrons and Positrons by neutral Atoms) code developed by Salvat et al. [41], which uses the Dirac partial-wave approach including relativistic corrections to calculate the electron elastic scattering by a local central interaction potential representing atoms. To perform the calculation in the optical potential formalism, we considered the Fermi nucleus distribution, the Dirac–Fock electron distribution, the Furness–McCarthy exchange potential, the correlation-polarization potential with the local density approximation, and the LDA absorption potential, described in detail in Ref. [41].

In our study, we observed that including the interference terms gives good agreement with reference data at small scattering angles ($< 30°$), but results in a significant overestimation of integral cross sections (as shown later in Fig. 5). Consequently, we decided to employ the simple incoherent sum of atomic scattering amplitudes, following the AR approximation. This approach not only eliminates the need for renormalization to satisfy the optical theorem, but also significantly enhances the agreement between the total cross sections (TCSs) and the experimental data, as previously stated in [42].

Nevertheless, to enhance the accuracy of our calculations, we introduced slight adjustments to the free parameters of the scattering potential, specifically targeting an increase in the differential cross sections at small scattering angles. The two parameters involved are b_{pol} and A_{abs}, included in the correlation polarization potential and the absorption potential, respectively. The default values used in ELSEPA have been validated for noble gases and mercury, but they can be modified to better match experimental data. Notably, above the ionization threshold, a higher absorption strength increases the DCSs at small scattering angles while decreasing them at intermediate and large angles. As for the b_{pol} parameter, the DCSs at small angles are the highest when b_{pol} is the lowest and decrease with increasing b_{pol}.

By examining the impact of these two parameters on the DCS, we qualitative determined optimized values for b_{pol} and A_{abs}. Specifically, for energies below 500 eV, the value of b_{pol} is fixed at 0.01. As the energy approaches 1 keV, it linearly increases from 0.01 to 6.6. Beyond 1 keV, the expression $\sqrt{\frac{E\ (\mathrm{eV})-50\ \mathrm{eV}}{22\mathrm{eV}}}$ governs the behavior of b_{pol} for both molecules. Regarding the A_{abs} parameters for N_2, it decreased linearly from 2.5 at 12 eV to 2 at 400 eV. For O_2, A_{Abs} transitions from 2 at 12 eV to 3 at 70 eV, and then decreases back to 2 at 300 eV. For higher energies, A_{Abs} is set to 2 for both molecules, which corresponds to the default value proposed by ELSEPA.

It should be made clear that the cross sections for each constituent atom are calculated using the known first optically allowed excitation threshold [43] and atomic polarizability [44] of that atom, prior to the application of the screening corrected additivity rule. The bond distances are taken from the pubchem database of 3D molecular structures [37]. For N2, the bond length is 1.12 Å, while for O2, it is 1.23 Å [45].

2.3. Electronic excitation

The third process which is of great importance during electron slowing down in the atmosphere is the excitation of molecules by electron impact. This process plays an important role in determining the internal energy and state distribution of the gaseous molecules in the atmosphere, and is mainly responsible for the increase of the mean energy loss in the low energy region.

The treatment of excitation process in oxygen and nitrogen is based on the relativistic formulae of Porter et al. [46]. For optically forbidden discrete excitations the cross section σ_j^{exc} to a state j of electrons at energy T is given by :

$$\sigma_j^{exc,forbidden} = \frac{q_0 A\phi\left(2W_j/m\beta^2c^2\right)}{\left(m\beta^2c^2/2W_j\right)W_j^2} \tag{7}$$

Table 2
Excitation cross section parameters for use in formulas (7)–(8). Those marked with (∗) are from Porter et al. [46], while the remaining parameters are obtained through fitting data or other models, as described in the text. Excitation threshold energies come from Itikawa, and Porter et al. [46,48,49].

	Excitation					
	State	W_j (eV)	A	Ω	γ	ν
N_2	vib ν 1-3 (∗)	1.85	0.273	7	1	1
	vib ν 4-8 (∗)	2.15	0.241	9	1	1
	$A^3\Sigma_u^+$	6.169	0.04	1.51	7.37	12.12
	$B^3\Pi_g$	7.353	0.06	1.71	9.0	7.0
	$W^3\Delta_u$	7.362	0.08	1.77	5.63	11.5
	$B'^3\Sigma_u^-$	8.165	0.04	1.69	16.7	714
	$a'^1\Sigma_u^-$	8.399	0.01	1.56	15.0	13.1
	$a^1\Pi_g$	8.549	0.09	1.00	7.93	9.56
	$w^1\Delta_u$	8.89	0.01	1.05	16.4	9.6
	$C^3\Pi_u$	11.032	1.17	2.25	0.07	0.57
	$E^3\Sigma_g^+$ (∗)	11.875	0.048	3.00	3.00	1.
	$a''^1\Sigma_g^+$	12.255	0.15	1.59	0.32	0.9
	$b^1\Pi_u$	12.5	0.12	0.85	1.29	2.34
	$b'^1\Sigma_u^+$	13.3	0.25	0.06	1.03	2.63
	$c_4'^1\Sigma^+$	12.94	0.23	0.05	−1.1	4.05
O_2	$a_1\Delta_g$	0.98	0.11	2.23	0.7	9
	$b_1\Sigma_g^+$	1.63	0.008	2.01	1	6
	$A^3\Sigma_u^+$ (∗)	4.5	0.02	0.9	1	1
	$2B$	10.29	0.008	0.17	0.8	1.3
	LB	9.96	0.009	0.93	1.5	0.4
	$B^3\Sigma_u^-$	6.12	0.13	0.21	1.7	2

where

$$\phi\left(2W_j/m\beta^2c^2\right) = \frac{\left[1-\left(2W_j/m\beta^2c^2\right)^{\alpha}\right]^{\beta}}{\left(m\beta^2c^2/2W_j\right)^{\Omega-1}}$$

is a distortion factor and allows for variations from the asymptotic Bethe formula at low energies. $q_0 = 4\pi a_0^2 R^2$ and has the numerical value of $6.513 * 10^{-14}$ eV^{2}cm^2, a_0 being the Bohr radius and R the Rydberg energy. W_j is the threshold excitation energy of the jth states, and A, α, β and Ω are four adjustable parameters.

The second form used to represent the cross section of discrete allowed excitations and for the excitation of Rydberg states is more consistent with the asymptotic form of Born–Bethe theory, and is calculated according to:

$$\sigma_j^{exc,allowed} = \frac{q_0 A\phi\left(2W_j/m\beta^2c^2\right)}{\left(m\beta^2c^2/2W_j\right)W_j^2}\left\{\ln\left[4\left(\frac{m\beta^2c^2}{2W_j}\right)\frac{C_j}{(1-\beta^2)}+\mathrm{e}\right]-\beta^2\right\} \tag{8}$$

where $\phi\left(2W_j/m\beta^2c^2\right)$ is given by

$$\phi\left(2W_j/m\beta^2c^2\right) = \left[1-\left(\frac{2W_j}{m\beta^2c^2}\right)^{\alpha}\right]^{\beta}\Theta\left(\frac{m\beta^2c^2}{2W_j}-1\right)$$

with

$$\Theta\left(\frac{m\beta^2c^2}{2W_j}-1\right) = \begin{cases} 1, & m\beta^2c^2/2 \geq W_j \\ 0, & m\beta^2c^2/2 < W_j \end{cases} \tag{9}$$

We determined the free parameters in Eqs. (7)–(8) (A, α, β and Ω) for most of the excitation states through a non-linear least squares analysis of various experimental data sets, following the procedure outlined in [47]. In cases where literature data were unavailable, the values for the excitation parameters were taken from the study by Porter et al. [46]. The cross section parameters and formulas for the excitation of Rydberg states were also taken from the publication by Porter et al. Their formulas employ a method to calculate the A and W_j parameters for each Rydberg series, that takes into account the principal quantum number and the quantum defect associated with the specific state.

The excitation of three possible allowed states ($B^3\Sigma_u^-$, Longest Band-LB, Second Band-2B), three forbidden states ($b^1\Sigma_g^+$, $a^1\Delta_g$, $A^3\Sigma_u^+$), plus 21 Rydberg states (7 with principal quantum number equal to 3, 7 with principal quantum number equal to 4, and 7 cumulative for all higher lying members), was taken into account in the present study for oxygen.

For molecular nitrogen three allowed levels ($b^1\Pi_u$, $b'^1\Sigma_u^+$, $c_4'^1\Sigma^+$), twelve forbidden levels (vib ν 1–3, vib ν 4–8, $A^3\Sigma_u^+$, $B^3\pi_g$, $W^3\Delta_u$, $B'^3\Sigma_u^-$, $a'^1\Sigma_u^-$, $w^1\Delta_u$, $C^3\Pi_u$, $E^3\Sigma_g^+$, $a^1\Pi_g$, $a''^1\Sigma_g^+$), plus 18 Rydberg states (6 with principal quantum number equal to 3, 6 with principal quantum number equal to 4, and 6 cumulative for all higher lying members), have been included. The values of the forbidden and allowed excitation parameters used in the present study and partially based on Porter et al. are listed in Table 2. For the parameters related to the excitation of Rydberg states, please refer to [46].

For the use of such a model for simulation purposes, the excitation of Rydberg-like states that often leads to auto-ionization needs to be considered. Following the recommendations of Stolarski [50] and Watson [51], a 50% probability of auto-ionization should be assumed when the excitation energy of a Rydberg state is greater than the ionization threshold for the material.

3. Results and discussion

We implemented the described models in C++, with the aim of interfacing them with Geant4-DNA in the near future. The computation of ionization and excitation cross sections is performed using their analytical formulations. As for elastic cross sections, we have employed interpolated cross section data tables, following the approach commonly used in particle transport codes.

3.1. Cross sections

3.1.1. Differential ionization cross section

For a given incident energy, the sum of Eq. (2) over all molecular orbitals gives the energy differential ionization cross-section. This has been evaluated at impinging electron energies varying from 10 eV to 1 MeV employing the RBEB formulation. In Fig. 1, the results are compared with the experimental cross sections from Opal et al. [52], Shyn [53,54], DuBois and Rudd [55], and the theoretical data from Pal et al. [56], computed by using the Jain–Khare semiempirical approach [57]. The differential cross sections reveal a good agreement with the experimental values and better than those determined from the Jain–Khare method. The main differences are observed for an incident

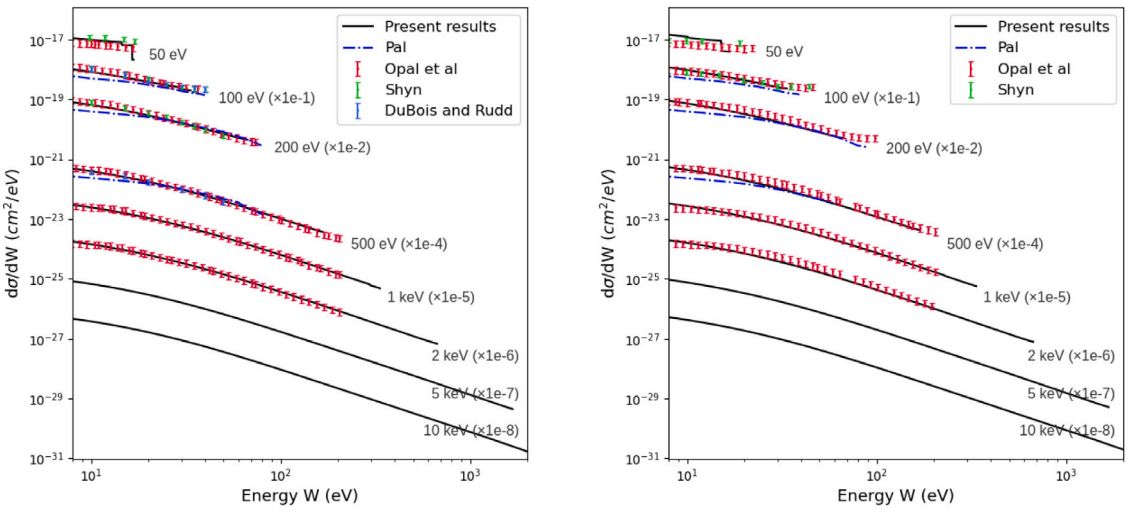

(a) N_2 (b) O_2

Fig. 1. Differential cross sections for ionization by electrons in molecular nitrogen (a) and oxygen (b) as a function of the ejected electron energy W, for several incident electron energies from the RBEB model (solid black lines). To improve the readability of the plot, the DCS results are presented only in the energy range of 50 eV to 10 keV (no experimental data are available in the literature for energies higher than 2 keV). Experimental data from Opal et al. [52], Shyn and Sharp [53], Shyn [54], and Du Bois and Rudd [55] are shown in symbols with their uncertainties; the semi-empirical data from Pal et al. [56] are shown in dash–dot blue line. (For interpretation of the references to color in this figure legend, the reader is referred to the web version of this article.)

electron energy of 50 eV, for which there is also strong disagreement between Shyn's and Opal's experimental data (about 50%).

3.1.2. Differential elastic cross sections

The elastic DCSs for electron scattering by N_2 and O2, obtained using the SCAR model with the proposed expression for b_{pol} and A_{abs}, are presented in Figs. 2–3. These results are compared with the ones obtained using the AR model, employing the default expression parameters from ELSEPA, as well as experimental data.

It is observed that the SCAR corrections lead to a decrease in the DCSs across the entire scattering angle range and particularly for energies below 200 eV, for both molecules. This correction significantly improves the agreement between the calculated DCSs and the experimental data, even at energies as low as 15 eV. The modified potential parameters increase the DCSs at zero angles by 4% to 34% for energies higher than about 50 eV, while improving the overall shape of the DCSs at energies below 300 eV. At high energies, our elastic model yields good results in reasonable agreement with the experimental data. In the case of oxygen, a slight underestimation of the DCSs at angles lower than 20° is observed when compared to the experimental data from Iga et al. [58], and Daimon et al. [59]. This discrepancy becomes more pronounced in the energy range of 100–500 eV. However, these results are reflected in higher TCS compared to other experimental findings, as will be discussed later.

3.1.3. Excitation cross sections

In Fig. 4 the excitation cross sections for each of the levels included in the present study are shown, along with experimental or semi-empirical data used for the fitting procedure. The cross sections trend at low energies and for the lower states is mainly based on the values recommended by Itikawa [48,49]. In the absence of experimental data in the intermediate-high energy range, the asymptotic dependence was obtained through data transcribed from S.F. Biagi's FORTRAN code (MagBoltz, versions 8.9 and later) [73,74] and the semi-empirical BEf-scaling results [75–77] for the dipole-allowed transitions.

3.1.4. Total cross sections

The total scattering cross section σ^{tot} of electrons at energy T in nitrogen and oxygen was calculated as $\sigma^{tot} = \sigma^{ion} + \sigma^{el} + \sigma^{exc}$ and can be compared in Fig. 5 with the recommended values by Itikawa and other cross section results. The individual contributions of ionization, excitation, and elastic processes are presented in solid lines, alongside experimental data and semi-empirical calculations (further details in the plot legend).

As expected, the excitation σ_{exc} and ionization σ_{ion} cross sections exhibit similar energy dependence for energies above approximately 200 eV, but σ_{exc} increases with decreasing energy due to the contribution of excitation to optically forbidden states. A glance at the figures shows that the high values of the elastic cross section, compared to those of other interaction effects, are remarkable at energies smaller than 100 eV.

The elastic cross section results demonstrate good agreement with all experimental data sets for N_2. For oxygen, small deviations are noticed for energies below 60 eV [48,81]. Nevertheless, these deviations are still within the range of Itakawa's experimental uncertainties (± 20%, not displayed in the plot).

The results obtained from the IAM-SCAR model are included for comparison in Fig. 5. As previously mentioned, the inclusion of the interference term in (6) leads to an overall increase in the integral elastic cross section across the entire energy range. Specifically, this enhancement is about 26% and 24% at 100 eV for N_2 and O_2, respectively, and decreases to 15% and 10% at 10 keV. It is worth noting that the experimental values from Iga et al. [58], and Daimon et al. [59] for O_2 demonstrate better agreement with the IAM-SCAR model compared to the AR-SCAR approximation. This overestimation of the TCS when compared to more recent experimental data is also reflected in their small-angle DCSs in Fig. 3, that show higher values in comparison to the predictions of the AR-SCAR model.

In Fig. 5 the excitation cross sections obtained in the present study are compared with those obtained using Porter's default parameters. For oxygen, the fitting procedure based on the most recent cross section

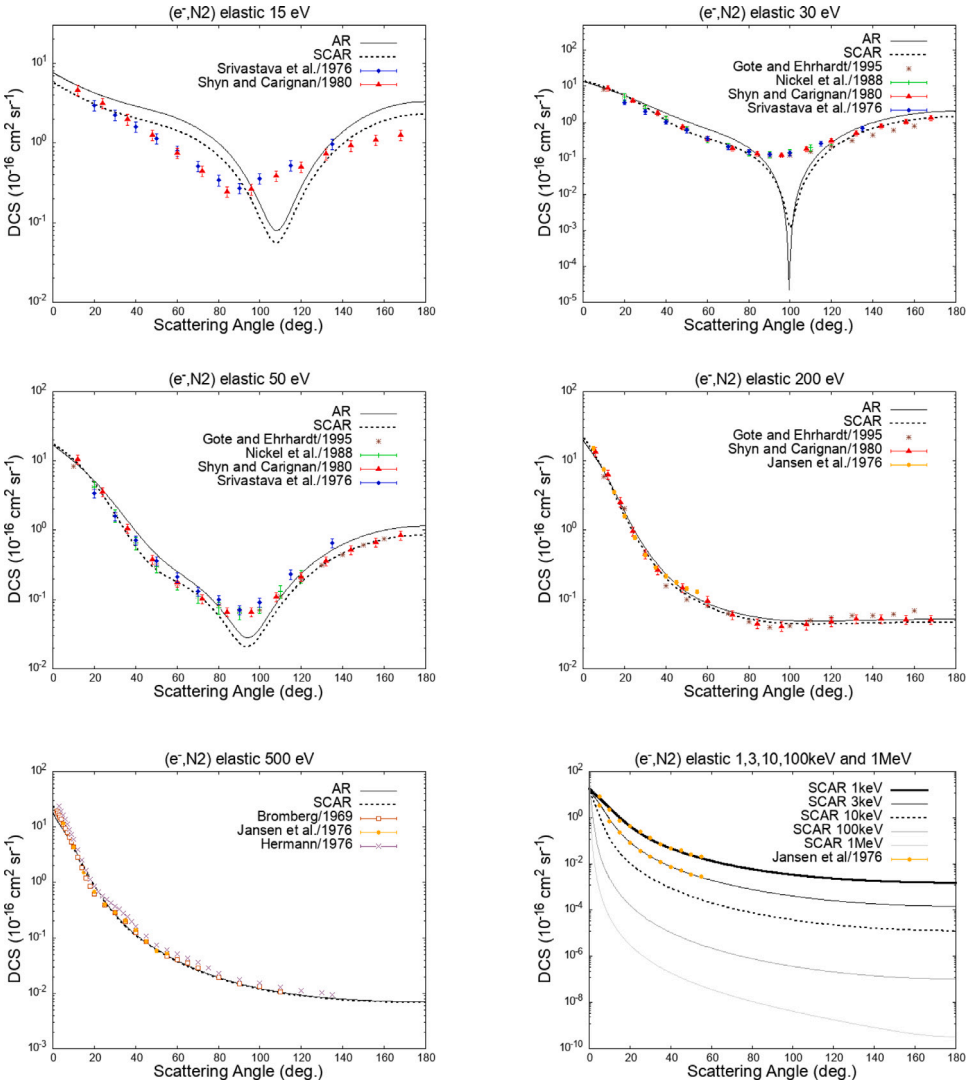

Fig. 2. Differential cross sections for the elastic scattering of electrons from nitrogen at energies 15, 30, 50, 200 eV; 0.5, 1, 3, 10, 100 keV and 1 MeV, obtained by applying the AR and SCAR models to the atomic results from the ELSEPA code. Experimental data are from: Gote and Ehrhardt [60], Shyn and Carignan [61], Srivastava et al. [62], Nickel et al. [63], Jansen et al. [64], Herrmann [65] and Bromberg [66].

measurements allows for a better description of the cross section at very low energies, while maintaining the same behavior at intermediate and high energies. As for nitrogen, our results show lower values compared to Porter's results, but they are in better agreement with the comprehensive set of surveyed excitation cross sections by Majeed and Strickland [82].

The total and partial cross sections for nitrogen obtained in the present study are compared with Grosswendt's results (dash–dot lines in Fig. 5), whose models are extensively described in [83–85]. TCSs are in good agreement with each other for energies higher than 1 keV, although the individual contributions of different processes are different. Grosswendt employs the non-relativistic version of the RBEB, which leads to an underestimation of the ionization cross section at high energies, and an empirical screened Rutherford formula to describe the elastic process. The excitation cross section used by Grosswendt is based on the formulas and cross section parameters of Porter et al. They introduced modifications to Porter's parameter to enhance excitation cross sections across the entire energy range, aiming to improve agreement with experimental TCS measurements. In line with this goal, they incorporated an extra excitation contribution to the cross section shape, which results in the 20 eV peak [83]. It is worth noting that the Grosswendt's cross-sections for N_2, already used in the PTra code developed at PTB, have recently been implemented in the Geant4-DNA toolkit [86].

The comparison of our results with other TCS experimental data and theoretical calculations demonstrates an overall good agreement. However, it is important to highlight some additional considerations. Firstly, the RBEB model employed in this study tends to overestimate the ionization cross section, particularly at lower energies and near the peak. This overestimation may arise from the approximation used, which does not account for differential oscillator strengths, as previously discussed by Bug et al. [85]. Secondly, the contribution of the excitation cross section also introduces a degree of uncertainty. For nitrogen, Itikawa does not provide recommended cross sections for the excitation of higher allowed states (i.e., those with thresholds above

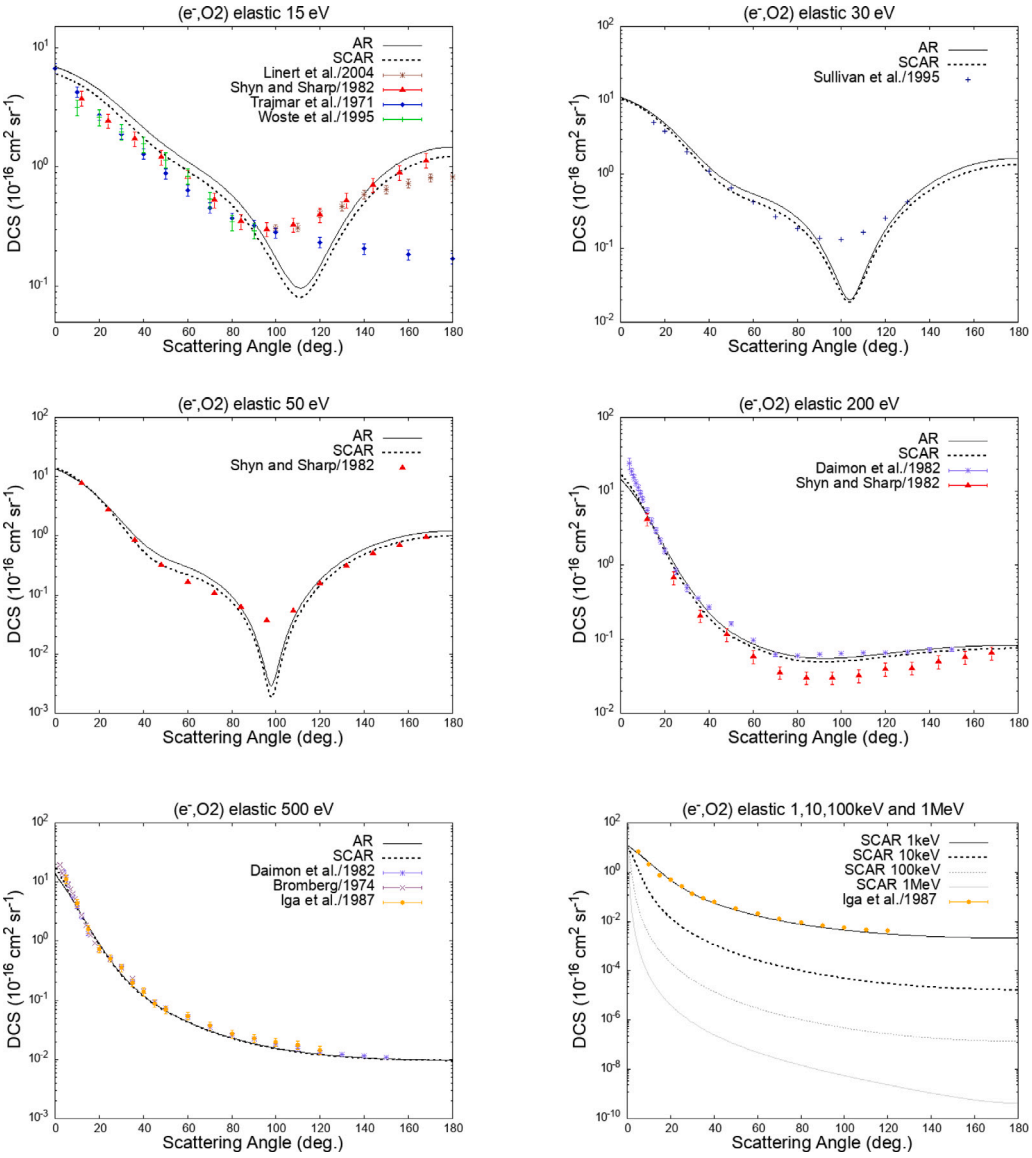

Fig. 3. Differential cross sections for the elastic scattering of electrons from oxygen at energies 15, 30, 50, 200 eV; 0.5, 1, 10, 100 keV and 1 MeV, obtained by applying the AR and SCAR models to the atomic results from the ELSEPA code. Experimental data are from: Linert et al. [67], Shyn and Sharp [68], Trajmar et al. [69], Woste et al. [70], Sullivan et al. [71], Iga et al. [58], Bromberg [72], and Daimon et al. [59].

12.5 eV), which exhibit large cross sections even at high electron energies. Due to the limited availability of measured values, the Rydberg cross section is also a major source of uncertainty. Lastly, it is important to note that most of the recommended data for forbidden excitation processes have large uncertainties, typically ranging from 25% to 40%. This reflects significant differences in the differential cross sections measured by different research groups.

3.2. Stopping power

To test the consistency of the presented interaction cross sections, we evaluated the electron stopping power from the analytical cross sections' models.

Assuming that an electron of initial energy E loses its energy only through exciting and ionizing collisions, the analytical mass stopping power can be written as

$$-(dE/dx) = -(dE/dx)^{ion} - (dE/dx)^{ex} \tag{10}$$

where the pathlength increment dx is expressed in mass units (i.e., in g/cm^2). The first term is given by

$$-(dE/\rho dx)^{ion} = n/\rho \sum_i \int_{B_i}^{(E+B_i)/2} W \frac{d\sigma_i^{ion}}{dW}(E)\, dW \tag{11}$$

where $\frac{d\sigma_i^{ion}}{dW}(E)$ is the energy-loss cross section for the ith ionization shell (with B_i its binding energy) for an incident electron of energy E losing an energy equal to W per unit of length, ρ is the density of the traversed medium and n is the number of molecules per unit of volume. For the second term of the stopping power, which is due to electronic excitations of the target, we have

$$-(dE/\rho dx)^{ex} = n/\rho \sum_i \sigma_i^{ex}(E) W_i \tag{12}$$

where $\sigma_i^{ex}(E)$ and W_i are the excitation cross section and the excitation threshold energy for the ith electronic excited state of the target, respectively. By substituting in Eqs. (11)–(12) the forms of cross sections

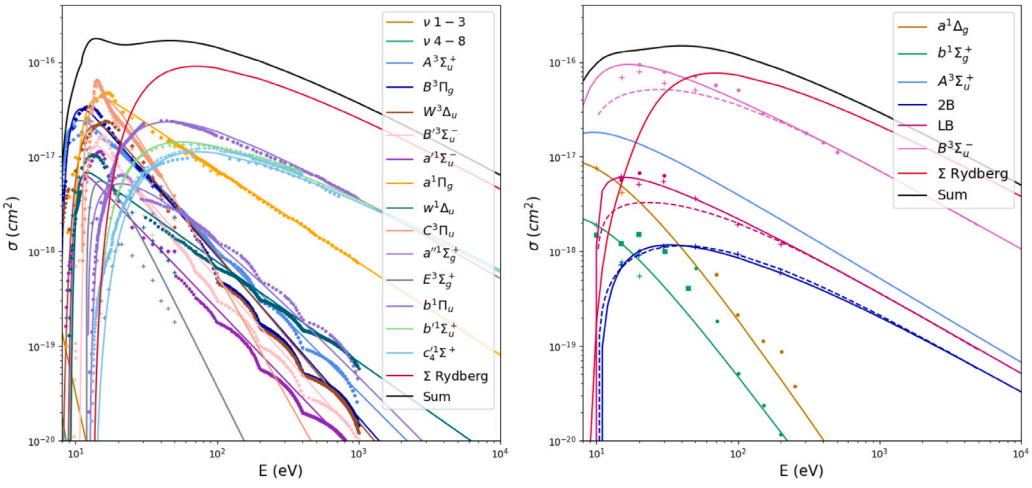

(a) N_2 (b) O_2

Fig. 4. Excitation cross sections for nitrogen (a) and oxygen (b) molecules obtained from Porter's formula with the parameters given in Table 2. To improve the readability of the plot, the DCS results are presented only in the energy range of 10 eV to 10 keV. The excitation cross sections for nitrogen are compared with experimental values from Itikawa (crosses) [49] and data from S.F. Biagi (dots) [73,74]. The excitation cross sections for oxygen are compared with experimental data from Itikawa (crosses) [48], Wakiya (dots) [78], Trajmar et al. (squares) [79], Linder and Schmidt (asterisks) [80] and semi-empirical BEf-scaling (dashed lines) results from [76]. The sums over all the Rydberg states for both molecules are also shown.

presented in the previous paragraph (Eqs. (1)–(7)–(8)), the electron stopping power was calculated in the incident energy range from 10 eV to 1 MeV.

In Fig. 6(a), the calculated mass stopping power values for nitrogen are presented. These values are compared with the semi-empirical formula of Peterson and Green [89], the Gümüş model [90], and the values from the NIST ESTAR database [43], based on ICRU report 37 [21]. For energies higher than 30 eV, the results show agreement within 10% with the data predicted by Peterson and Green, as well as those by Majeed and Strickland. It should be noted that our results slightly overestimate the stopping power in comparison to the NIST values. This discrepancy is likely due to the RBEB model overestimating the impact ionization cross sections, in contrast to the recommended values by Itikawa (as discussed in Bug et al. [85]). Nevertheless, the agreement between our results and the NIST values remains good, with differences within 6% across the entire energy range. For energies lower than 30 eV there seems to be a lack of contribution to energy loss. To improve the agreement, a few corrections and extensions to electronic excitation states could be applied, as discussed by Grosswendt et al. [83].

In Fig. 6(b), the mass stopping power values for oxygen are compared with Peterson and Green's semi-empirical formula, Gümüş's model [90], Gupta's results [91], energy loss measurements from Majeed [82], and values from NIST's ESTAR database. A very good agreement is observed with the recommended values by NIST, with relative differences of 3.5% across the entire energy range. As for the other stopping power data, better agreement is obtained with Gupta and Majeed's predictions, showing relative differences of about 5% for energies ranging from 30 eV to 1 keV, and less than 10% for higher energies. It could be noted that the calculated stopping power is significantly underestimated for energies below 20–30 eV, and the same consideration made in the case of nitrogen could be applied.

The stopping power values obtained by Gumus are in good agreement with the intermediate and high energy data in the ESTAR database and seems to better reproduce energy loss in the very low energy range, given also the good agreement with Peterson's results. Nevertheless, Gumus' model is not derived from cross-section models but is based on a modified version of Rohrlich and Carlson's formula for collision stopping power [92,93]. This makes it inapplicable for simulation purposes. In this context, the results obtained with the proposed models in the analyzed energy range represent an excellent set of cross sections to be used for Monte Carlo applications.

4. Conclusions and perspectives

The ions produced by cosmic rays in different ionization states and spatial distribution can significantly change chemical reaction rates by orders of magnitude. Physics models for electron impact on oxygen and nitrogen molecules to be used in event-by-event Monte Carlo simulations are a necessary starting point to calculate the ionization state, the concentration and the spatial distribution of the ions produced by cosmic rays interaction with molecules in the atmosphere. In this paper, we have presented models (elastic scattering, electronic excitation and ionization processes) for electron transport in molecular oxygen and nitrogen that are applicable over a wide energy range (10 eV - 1 MeV).

We evaluated these cross section models by comparing them with experimental data, obtaining an overall good agreement. A second validation was performed by comparing the analytically calculated stopping power with values from the NIST database and from other calculation methodologies. The good agreement of the stopping power results demonstrates the applicability of the cross-section models across the entire energy range studied here.

Further work is underway to exploit these new cross sections in Monte Carlo code using a Track-Structure approach for simulation applications. Specifically, we are working on integrating these models into Geant4-DNA to simulate the ionization effects in small volumes at different altitudes in the Earth's troposphere and stratosphere.

The extension of Geant4-DNA to simulate physics for any molecule of climatological interest opens up for the first time the possibility to accurately simulate the complicated physicochemical processes involved in the atmosphere. Besides atmospheric applications, having a complete set of low-energy electromagnetic interactions with gaseous molecules may also be of great interest for various applications such as modeling discharge phenomena, radiation chemistry, micro and nano dosimetry experiments, and exobiology studies.

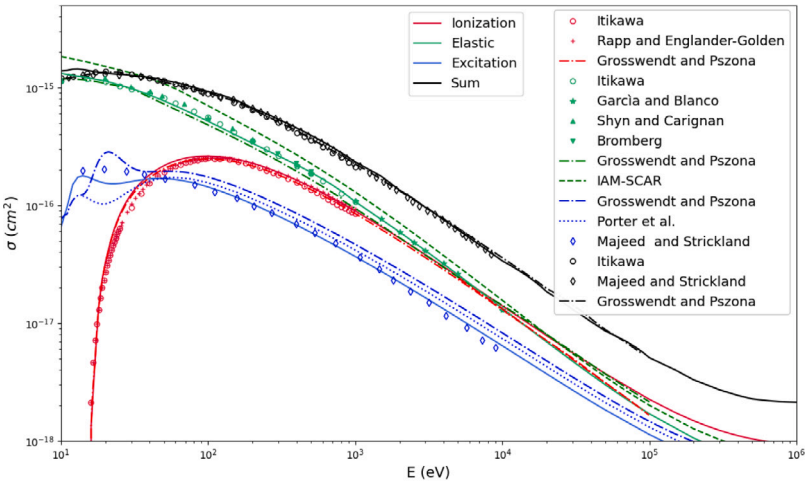

(a) N_2

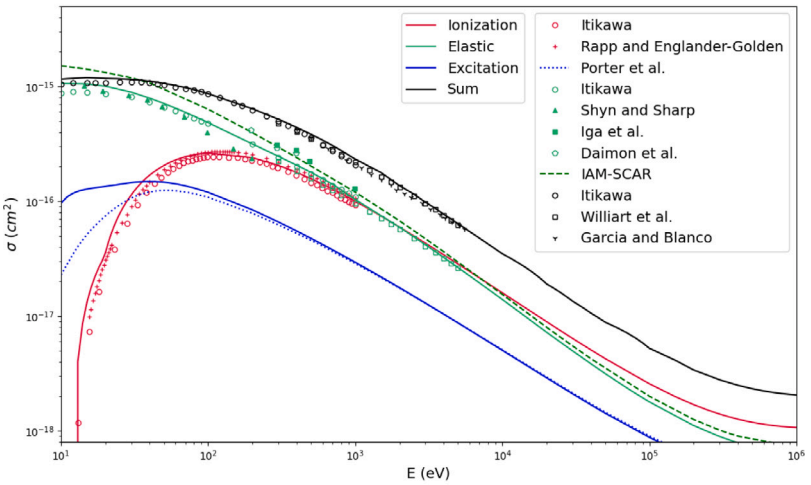

(b) O_2

Fig. 5. Cross section for electrons in nitrogen (a) and oxygen (b) plotted as a function of electron incident energy for elastic scattering (green), electron excitation (blue), ionization (red), and total (black). The results obtained in the present study for excitation, elastic, ionization and total cross section are presented in solid lines. These are compared with values from Grosswendt and Pszona [83], Porter et al. [46], Majeed and Strickland [82], Itikawa [48,49], Williart et al. [81], Garcá and Blanco [87], Iga et al. [58], Shyn et al. [61,68], Bromberg [66], Daimon et al. [59], and Rapp and Englander-Golden [88]. (For interpretation of the references to color in this figure legend, the reader is referred to the web version of this article.)

Acronyms

NIST	National Institute of Standards and Technology
ICRU	International Commission on Radiation Units and Measurements
ESTAR	Stopping Powers and Ranges for Electrons
MC	Monte Carlo
MC-TS	Monte Carlo Track Structure
Geant4	GEometry ANd Tracking
RBEB	Relativistic Binary Encounter Bethe
IAM	Independent Atom Model
AR	Additivity Rule
SCAR	Screening Corrected Additivity Rule
ELSEPA	Elastic Scattering of Electrons and Positrons by neutral Atoms
TCS	Total Cross Section
DCS	Differential Cross Section

Declaration of competing interest

The authors declare that they have no known competing financial interests or personal relationships that could have appeared to influence the work reported in this paper.

Acknowledgments

This project has been partially funded by Programma Operativo Nazionale (PON) “Ricerca e Innovazione” 2014–2020 (Decree 1061/2021) Action IV.5 “Dottorati su tematiche Green”.

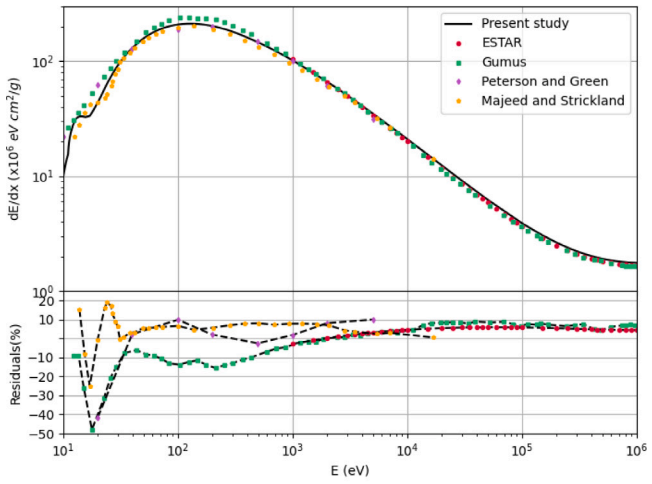

(a) N_2

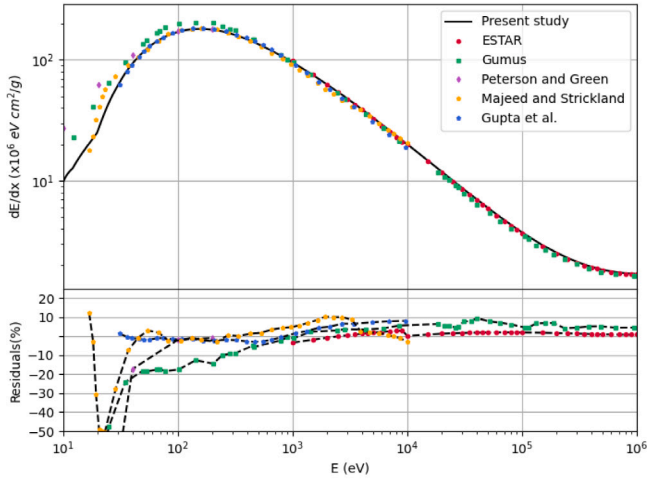

(b) O_2

Fig. 6. Energy dependence of the electronic mass stopping power in nitrogen (a) and oxygen (b) calculated using Eq. (10). Present calculations (solid black line) are compared with semi-empirical formula of Peterson and Green (purple) [89], Gümüş model (green) [90], semi-empirical formula from Gupta et al. (blue) [91], energy loss measurements from Majeed and Strickland [82], and data from NIST ESTAR database (red) [43]. The relative differences between present analytical results and the other data is shown in the bottom panel of the two figures. (For interpretation of the references to color in this figure legend, the reader is referred to the web version of this article.)

References

[1] Burkholder JB, Abbatt JPD, Barnes I, Roberts JM, Melamed ML, Ammann M, et al. The essential role for laboratory studies in atmospheric chemistry. Environ Sci Technol 2017;51:2519–28. http://dx.doi.org/10.1021/acs.est.6b04947.

[2] Futrell JH, T.O. Tiernan. Ion-molecule reactions. Science 1968;162(3852):415–22. http://dx.doi.org/10.1126/science.162.3852.415.

[3] Kinetic Database for Astrochemistry: KIDA. https://kida.astrochem-tools.org/.

[4] Satta M, Castrovilli MC, Nicolanti F, Casavola AR, Mancini TC, Cartoni A. Perspectives of gas phase ion chemistry: Spectroscopy and modeling. Condens Matter 2022;7(3):46. http://dx.doi.org/10.3390/condmat7030046.

[5] Cartoni A, Catone D, Bolognesi P, Satta M, Markus P, Avaldi L. HSO_2^+ formation from ion-molecule reactions of SO_2^+ with water and methane: two fast reactions with reverse temperature-dependent kinetic trend. HOT Paper Chem Eur J 2017;23:6772–80. http://dx.doi.org/10.1002/chem.201700028.

[6] Satta M, Cartoni A, Catone D, Castrovilli MC, Bolognesi P, Zema N, et al. The reaction of sulfur dioxide radical cation with hydrogen and its relevance in solar geoengineering models. ChemPhysChem 2020;21:1146–56. http://dx.doi.org/10.1002/cphc.202000194.

[7] Ravishankara AR, Daniel JS, Portmann RW. Nitrous oxide (N_2O): the dominant ozone-depleting substance emitted in the 21st century. Science 2009;326(5949):123–5. http://dx.doi.org/10.1126/science.1176985.

[8] Portmann RW, Daniel JS, Ravishankara AR. Stratospheric ozone depletion due to nitrous oxide: influences of other gases. Philos Trans R Soc London [Biol] 2012;367(1593):1256–64. http://dx.doi.org/10.1098/rstb.2011.0377.

[9] Müller R. The impact of the rise in atmospheric nitrous oxide on stratospheric ozone. Ambio 2021;50(1):35–9. http://dx.doi.org/10.1007/s13280-020-01428-3.

[10] Incerti S, Kyriakou I, Bernal MA, Bordage MC, Francis Z, Guatelli S, et al. Geant4-DNA example applications for track structure simulations in liquid water: A report from the Geant4-DNA project. Med Phys 2018;45:e722–39. http://dx.doi.org/10.1002/mp.13048.

[11] Bernal MA, Bordage MC, Brown JMC, Davídková M, Delage E, El Bitar Z, et al. Track structure modeling in liquid water: A review of the Geant4-DNA very low energy extension of the Geant4 Monte Carlo simulation toolkit. Phys Med 2015;31:861–74. http://dx.doi.org/10.1016/j.ejmp.2015.10.087.

[12] Incerti S, Baldacchino G, Bernal M, Capra R, Champion C, Francis Z, et al. The Geant4-DNA project. Int J Model Simul Sci Comput 2010;1:157–78. http://dx.doi.org/10.48550/arXiv.0910.5684.

[13] Incerti S, Ivanchenko A, Karamitros M, Mantero A, Moretto P, Tran HN, et al. Comparison of Geant4 very low energy cross section models with experimental data in water. Med Phys 2010;37:4692–708. http://dx.doi.org/10.1118/1.3476457.

[14] Agostinelli S, et al. GEANT4 - A simulation toolkit. Nucl Instrum Methods A 2003;506:250–303. http://dx.doi.org/10.1016/S0168-9002(03)01368-8.

[15] Allison J, et al. Geant4 developments and applications. IEEE Trans Nucl Sci 2006;53:270–8. http://dx.doi.org/10.1109/TNS.2006.869826.

[16] Allison J, et al. Recent developments in GEANT4. Nucl Instrum Methods A 2016;835:186–225. http://dx.doi.org/10.1016/j.nima.2016.06.125.

[17] Shin WG, Ramos-Mendez J, Tran NH, Okada S, Perrot Y, Villagrasa C, et al. Geant4-DNA simulation of the pre-chemical stage of water radiolysis and its impact on initial radiochemical yields. Phys Med 2021;88:86–90. http://dx.doi.org/10.1016/j.ejmp.2021.05.029.

[18] Chappuis F, Grilj V, Tran HN, Zein SA, Bochud F, Bailat C, et al. Modeling of scavenging systems in water radiolysis with Geant4-DNA. Phys Med 2023;108:102549. http://dx.doi.org/10.1016/j.ejmp.2023.102549.

[19] Hoyle CR, Fuchs C, Järvinen E, Saathoff H, Dias A, El Haddad I, et al. Aqueous phase oxidation of sulphur dioxide by ozone in cloud droplets. Atmos Chem Phys 2016;16:1693–712. http://dx.doi.org/10.5194/acp-16-1693-2016.

[20] Voigtländer J, Duplissy J, Rondo L, Kürten A, Stratmann F. Numerical simulations of mixing conditions and aerosol dynamics in the CERN CLOUD chamber. Atmos Chem Phys 2012;12(4):2205–14. http://dx.doi.org/10.5194/acp-12-2205-2012.

[21] ICRU. Stopping powers for electrons and positrons. Report no. 37, Bethesda, MD: International Commission on Radiation Units and Measurements; 1984, http://dx.doi.org/10.1093/jicru/os19.2.Report37.

[22] Kim Y, Santos J, Parente F. Extension of the binary-encounter-dipole model to relativistic incident electrons. Phys Rev A 2000;62:052710. http://dx.doi.org/10.1103/PhysRevA.62.052710.

[23] Kim YK, Rudd ME. Binary-encounter-dipole model for electron-impact ionization. Phys Rev A 1994;50:3954–67. http://dx.doi.org/10.1103/PhysRevA.50.3954.

[24] Tessaro VB, Gervaisc B, Poignantb F, Beuveb M, Galassi ME. Monte Carlo transport of swift protons and light ions in water: The influence of excitation cross sections, relativistic effects, and Auger electron emission in w-values. Phys Med 2021;88:71–85. http://dx.doi.org/10.1016/j.ejmp.2021.06.006.

[25] Kim YK. Total ionization cross sections of molecules by electron impact. In: Christophorou LG, Olthoff JK, Vassiliou P, editors. Gaseous dielectrics X. Boston, MA: Springer; 2004, http://dx.doi.org/10.1007/978-1-4419-8979-6_1.

[26] Hwang W, Kim YK, Rudd ME. New model for electron impact ionization cross sections of molecules. J Chem Phys 1996;104:2956. http://dx.doi.org/10.1063/1.471116.

[27] Edel S. Modelisation du Transport des Photons et de s'Electrons Dans l'ADN Plasmide (Ph.D. thesis), Toulouse, France: Universite Toulouse III-Paul Sabatier; 2006, https://theses.hal.science/tel-01998577/document.

[28] Santos JP, et al. Cross sections for K-shell ionization of atoms by electron impact. J Phys B: At Mol Opt Phys 2003;36:4211. http://dx.doi.org/10.1088/0953-4075/36/21/002.

[29] Hwang W, Kim YK, Rudd ME. New model for electron-impact ionization cross sections of molecules. J Chem Phys 1996;104:2956–66. http://dx.doi.org/10.1063/1.471116.

[30] Jolly WL, Bomben KD, Eyermann CJ. Core-electron binding energies for gaseous atoms and molecules. At Data Nucl Data Tables 1984;31:411. http://dx.doi.org/10.1016/0092-640X(84)90011-1.

[31] Massey HSW, Burhop EHS, Gilbody HB. Atomic scattering: Electronic and ionic impact phenomena. 2nd ed. 1969, p. 2, https://www.science.org/doi/10.1126/science.168.3930.462.b.

[32] Blanco F, García G. Screening corrections for calculation of electron scattering from polyatomic molecules. Phys Lett A 2003;317:458. http://dx.doi.org/10.1016/j.physleta.2003.09.016.

[33] Blanco F, García G. Screening corrections for calculation of electron scattering differential cross sections from polyatomic molecules. Phys Lett A 2004;330:230. http://dx.doi.org/10.1016/j.physleta.2004.07.027.

[34] Sanz AG, Fuss MG, Blanco F, Gorfinkiel JD, Almeida D, Ferreira da Silva F, et al. An investigation into electron scattering from pyrazine at intermediate and high energies. J Chem Phys 2013;139:184310. http://dx.doi.org/10.1063/1.4829771.

[35] Milosavljević AR, et al. Absolute cross sections for elastic electron scattering from 3-hydroxytetrahydrofuran. New J Phys 2008;10:103005. http://dx.doi.org/10.1088/1367-2630/10/10/103005.

[36] Maljkovic JB, Milosavljevic AR, Blanco F, Šević D, García G, Marinkovic BP. Phys Rev 2009;A79:052706. http://dx.doi.org/10.1103/PhysRevA.79.052706.

[37] Blanco F, García G. Screening corrections for calculation of electron scattering from polyatomic molecules. Phys Lett A 2003;317:458–62. http://dx.doi.org/10.1016/j.physleta.2004.07.027.

[38] Fuss MC, Sanz AG, Blanco F, Limão-Vieira P, Brunger MJ, García G. Differential and integral electron scattering cross sections from tetrahydrofuran (THF) over a wide energy range: 1-10000 eV. Eur Phys J D 2014;68(6). https://www.researchgate.net/publication/273568027.

[39] Raj D. A note on the use of the additivity rule for electron-molecule elastic scattering. Phys Lett A 1991;160:6–9. http://dx.doi.org/10.1016/0375-9601(91)91070-T.

[40] Blanco F, Ellis-Gibbings L, García G. Screening corrections for the interference contributions to the electron and positron scattering cross sections from polyatomic molecules. Chem Phys Lett 2016;64571–5. http://dx.doi.org/10.1016/j.cplett.2015.11.056.

[41] Salvat F, Jablonski A, Powell CJ. ELSEPA—Dirac partial-wave calculation of elastic scattering of electrons and positrons by atoms, positive ions and molecules. Comput Phys Commun 2005;165:157–90. http://dx.doi.org/10.1016/j.cpc.2020.107704.

[42] Demes S, Kelemen V, Remeta EY. Elastic electron scattering by the CF_3 radical in the 1–1000 eV energy range. J Phys B: At Mol Opt Phys 2017;50(13):135201. http://dx.doi.org/10.1088/1361-6455/aa739f.

[43] NIST. ESTAR database, URL https://physics.nist.gov/PhysRefData/Star/Text/ESTAR.html.

[44] Computational Chemistry Comparison and Benchmark DataBase Release 22 (May 2022) Standard Reference Database 101. https://cccbdb.nist.gov/pollistx.asp.

[45] PubChem. PubChem database. 2019, https://pubchem.ncbi.nlm.nih.gov.

[46] Porter HS, Jackman CH, Green AES. Efficiencies for production of atomic nitrogen and oxygen by relativistic proton impact in air. J Chem Phys 1976;65:154. http://dx.doi.org/10.1063/1.432812.

[47] Green AES, Stolarski RS. Analytic models of electron impact excitation cross sections. J Atm Terrest Phys 1972;54:1703–17. http://dx.doi.org/10.1016/0021-9169(72)90030-X.

[48] Itikawa Y. Cross sections for electron collisions with oxygen molecules. J Phys Chem Ref Data 2009;38(1):1–20. http://dx.doi.org/10.1063/1.3025886.

[49] Itikawa Y. Cross sections for electron collisions with nitrogen molecules. J Phys Chem Ref Data 2006;35(1):31–53. http://dx.doi.org/10.1063/1.1937426.

[50] Stolarski RS, Green AES. Calculations of auroral intensities from electron impact. J Geophys Res 1967;72(15):3967–74. http://dx.doi.org/10.1029/JZ072i015p03967.

[51] Watson CE, Dulock VA, Stolarski RS, Green AES. Electron impact cross sections for atmospheric species: 3. Molecular oxygen. J Geophys Res 1967;72(15):3961–6. http://dx.doi.org/10.1029/JZ072i015p03961.

[52] Opal CB, Beaty EC, Peterson WK. Tables of secondary-electron-production cross sections. At Data 1972;4:209–53. http://dx.doi.org/10.1016/S0092-640X(72)80004-4.

[53] Shyn TW, Sharp WE. Doubly differential cross sections of secondary electrons ejected from molecular oxygen by electron impact. Phys Rev A 1991;43(5):2300–5. http://dx.doi.org/10.1103/PhysRevA.43.2300.

[54] Shyn TW. Doubly differential cross sections of secondary electrons ejected from gases by electron impact: 50–400 eV on N_2. Phys Rev A 1983;27(5):2388–95. http://dx.doi.org/10.1103/PhysRevA.27.2388.

[55] DuBois RD, Rudd ME. Absolute doubly differential cross sections for ejection of secondary electrons from gases by electron impact. II. 100-500-eV electrons on neon, argon, molecular hydrogen, and molecular nitrogen. Phys Rev A 1978;17(3):843–8. http://dx.doi.org/10.1103/PhysRevA.17.843.

[56] Pal S, Kumar J, Bhatt P. Electron impact ionization cross-sections for the N_2 and O_2 molecules. J Electron Spectrosc Relat Phenom 2003;129(1):35–41. http://dx.doi.org/10.1016/S0368-2048(03)00033-1.

[57] Jain DK, Khare SP. Ionizing collisions of electrons with CO_2, CO, H_2O, CH_4 and NH_3. J Phys B: At Mol Opt Phys 1976;9(8):1429–38. http://dx.doi.org/10.1088/0022-3700/9/8/023.

[58] Iga I, et al. Elastic differential cross section measurements for electron scattering from Ar and O_2 in the intermediate-energy range. J Phys B: Atom Mol Phys 1987;20:1095. http://dx.doi.org/10.1088/0022-3700/20/5/025.

[59] Daimon H, Hayashi S, Kondow T, Kuchitsu K. Measurements of differential cross sections of low-energy electrons elastically scattered by gas molecules. II. Scattering of 200–500 eV electrons by molecular oxygen. J Phys Soc Japan 1982;51(8):2641–9. http://dx.doi.org/10.1143/JPSJ.51.2641.

[60] Gote M, Ehrhardt H. Rotational excitation of diatomic molecules at intermediate energies: absolute differential state-to-state transition cross sections for electron scattering from N_2, Cl_2, CO and HCl. J Phys B: At Mol Opt Phys 1995;28:3957. http://dx.doi.org/10.1088/0953-4075/28/17/029.

[61] Shyn TW, Carignan GR. Angular distribution of electrons elastically scattered from gases: 1.5–400 eV on N_2. Phys Rev A 1980;22(3):923–9. http://dx.doi.org/10.1103/PhysRevA.22.923.

[62] Srivastava SK, Chutjian A, Trajmar S. Absolute elastic differential electron scattering cross sections in the intermediate energy region. II.— N_2. J Chem Phys 1976;64:1340. http://dx.doi.org/10.1063/1.432400.

[63] Nickel JC, Mott C, Kanik I, McCollum DC. Absolute elastic differential electron scattering cross sections for carbon monoxide and molecular nitrogen in the intermediate energy region. J Phys B: At Mol and Opt Phys 1988;21(10):1867–77, https://doi.10.1088/0953-4075/21/10/018.

[64] Jansen RHJ, Heer FJ, Luyken HJ, Wingerden B, Blaauw HJ. Absolute differential cross sections for elastic scattering of electrons by helium, neon, argon and molecular nitrogen. J Phys B: At Mol and Opt Phys 1976;9(2):185–212. http://dx.doi.org/10.1088/0022-3700/9/2/009.

[65] Herrmann D. Differential cross sections for elastic electron scattering. II. Charge cloud polarization in N_2. J Chem Phys 1976;64(1). http://dx.doi.org/10.1063/1.431951.

[66] Bromberg JP. Absolute differential cross sections of elastically scattered electrons. I. He, N_2, and CO at 500 eV. J Chem Phys 1969;50(9):3906. http://dx.doi.org/10.1063/1.1671647.

[67] Linert I, King GC, Zubek M. Measurements of differential cross sections for elastic electron scattering in the backward direction by molecular oxygen. J Phys B: At Mol and Opt Phys 2004;37(23):4681–91. http://dx.doi.org/10.1088/0953-4075/37/23/009.

[68] Shyn TW, Sharp WE. Angular distribution of electrons elastically scattered from O_2: 2.0-200 eV impact energy. Phys Rev A 1982;26(3):1369. http://dx.doi.org/10.1103/PhysRevA.26.1369.

[69] Trajmar S, Cartwright D, Williams W. Differential and integral cross sections for the electron-impact excitation of the $a^1\Delta_g$ and $b^1\Sigma_g^+$ states of O_2. Phys Rev A 1971;4(4):1482–92. http://dx.doi.org/10.1103/PhysRevA.4.1482.

[70] Woste G, et al. Differential and integral cross sections for elastic scattering of low-energy electrons by O_2. J Phys B: At Mol Opt Phys 1995;28:4141. http://dx.doi.org/10.1088/0953-4075/28/18/016.

[71] Sullivan JP, Gibson JC, Gulley RJ, Buckman SJ. Low-energy electron scattering from O_2. J Phys B: At Mol Opt Phys 1995;28:4319. http://dx.doi.org/10.1088/0953-4075/28/19/017.

[72] Bromberg JP. Absolute differential cross sections of elastically scattered electrons. V. O_2 and CO_2 at 500, 400, and 300 eV. J Chem Phys 1974;60(5):1717. http://dx.doi.org/10.1063/1.1681265.

[73] Lxcat. LXCat website, https://nl.lxcat.net/contributors/.

[74] Biagi SF. Monte Carlo simulation of electron drift and diffusion in counting gases under the influence of electric and magnetic fields. Nucl Instrum Methods A 1999;421(1–2):234–40. http://dx.doi.org/10.1016/S0168-9002(98)01233-9.

[75] Kim YK. Scaling of plane-wave Born cross sections for electron-impact excitation of neutral atoms. Phys Rev A 2001;64(3):032713. http://dx.doi.org/10.1103/PhysRevA.64.032713.

[76] Suzuki D, Kato H, Ohkawa M, Anzai K, Tanaka H, Limao-Vieira P, et al. Electron excitation of the Schumann–Runge continuum, longest band, and second band electronic states in O_2. J Chem Phys 2011;134(6):064311. http://dx.doi.org/10.1063/1.3533442.

[77] Brunger MJ, Thorn PA, Campbell L, Kato H, Kawahara H, Hoshino M, et al. Application of the BEf-scaling approach to electron impact excitation of dipole-allowed electronic states in molecules. J Phys Conf Ser 2008;115:012004. http://dx.doi.org/10.1088/1742-6596/115/1/012004.

[78] Wakiya K. Differential and integral cross sections for the electron impact excitation of O2. I. Optically allowed transitions from the ground state. J Phys B: Atom Mol Phys 1978;11:3913. http://dx.doi.org/10.1088/0022-3700/11/22/019.

[79] Trajmar S, Williams W, Kuppermann A. Angular dependence of electron impact excitation cross sections of O_2. J Chem Phys 1972;56:3759. http://dx.doi.org/10.1063/1.1677774.

[80] Linder F, Schmidt H. Experimental study of low energy e-O_2 collision processes. Z Natforsch A 1971;26(10):1617–25. http://dx.doi.org/10.1515/zna-1971-1008.

[81] Williart A, Kendall PA, Blanco F, Tegeder P, Garcia G, Mason NJ. Inelastic scattering and stopping power for electrons in O_2 and O_3 at intermediate and high energies, 0.3–5 keV. Chem Phys Lett 2003;375:39–44. http://dx.doi.org/10.1016/S0009-2614(03)00801-7.

[82] Majeed T, Strickl DJ. New survey of electron impact cross sections for photoelectron and auroral electron energy loss calculations. J Phys Chem Ref Data 1997;26:335–49. http://dx.doi.org/10.1063/1.556008.

[83] Grosswendt B, Pszona S. The track structure of α-particles from the point of view of ionization-cluster formation in ‘nanometric’ volumes of nitrogen. Radiat Environ Biophys 2002;41(2):91–102. http://dx.doi.org/10.1007/s00411-002-0144-9.

[84] Grosswendt B, Waibel E. Transport of low energy electrons in nitrogen and air. Nucl Instrum Methods 1978;155(1–2):145–56. http://dx.doi.org/10.1016/0029-554X(78)90198-2.

[85] Bug M, Gargioni E, Nettelbeck H, Baek W, Hilgers G, Rosenfeld A, et al. Ionization cross section data of nitrogen, methane, and propane for light ions and electrons and their suitability for use in track structure simulations. Phys Rev E 2013;88(4). http://dx.doi.org/10.1103/PhysRevE.88.043308.

[86] Pietrzak M, et al. Intercomparison of nanodosimetric distributions in nitrogen simulated with Geant4 and PTra track structure codes. Phys Med 2022;102:103–9. http://dx.doi.org/10.1016/j.ejmp.2022.09.003.

[87] García G, Blanco F. Energy dependence of the total cross section for electron scattering by N_2 and CO molecules at energies above 1 keV. Phys Lett A 2001;279:1–2. http://dx.doi.org/10.1016/S0375-9601(00)00822-7.

[88] Rapp D, Englander-Golden P. Total cross sections for ionization and attachment in gases by electron impact. I. Positive ionization. J Chem Phys 1965;43:1464. http://dx.doi.org/10.1063/1.1696957.

[89] Peterson LR, Green AES. The relation between ionization yields, cross sections and loss functions. J Phys B 1968;1:1131–40. http://dx.doi.org/10.1088/0022-3700/1/6/317.

[90] Gumus H. Simple stopping power formula for low and intermediate energy electrons. Rad Phys Chem 2005;72:7–12. http://dx.doi.org/10.1016/j.radphyschem.2004.03.006.

[91] Gupta P, Jhanwar BL, Khare SP. Stopping power of atmospheric gases for electrons. Physica B+C 1975;79B:311–21. http://dx.doi.org/10.1016/0378-4363(75)90098-4.

[92] Rohrlich F, Carlson BC. Positron–electron differences in energy loss and multiple scattering. Phys Rev 1954;93:38–44. http://dx.doi.org/10.1103/PhysRev.93.38.

[93] Sugiyama H. Stopping power formula for intermediate energy electrons. Phys Med Biol 1985;30:4331–5. http://dx.doi.org/10.1016/j.radphyschem.2004.03.006.